Elsevier Editorial System(tm) for Separation and Purification Technology
Manuscript Draft

Manuscript Number: SEPPUR-D-13-01457R1

Title: Synthesis and Characterization of Silica Gel - Polyacrylonitrile Mixed Matrix Forward Osmosis Membranes Based on Layer-by-Layer Assembly

Article Type: Full Length Article

Keywords: silica gel (SG); mixed matrix membrane (MMM); forward osmosis (FO); phase inversion; crosslinked layer-by-layer (xLbL) assembly; internal concentration polarization.

Corresponding Author: Dr. Chuyang Y. Tang, PhD

Corresponding Author's Institution: The University of Hong Kong

First Author: Jian-Yuan Lee

Order of Authors: Jian-Yuan Lee; Saren Qi ; Xin Liu; Ye Li; Fengwei Huo; Chuyang Tang

## Highlights

- Silica gel (SG) based mixed matrix membranes (MMM) were prepared as FO substrates.
- The MMM with 1 wt.% SG (M1.00) loading had improved porosity and water permeability.
- M1.00 showed reduced *S* value compared to the membrane without SG loading.
- M1.00 achieved high FO water flux of >100 $L/m^2h$ for 1 M $MgCl_2$ DS and 0-10 mM NaCl FS.

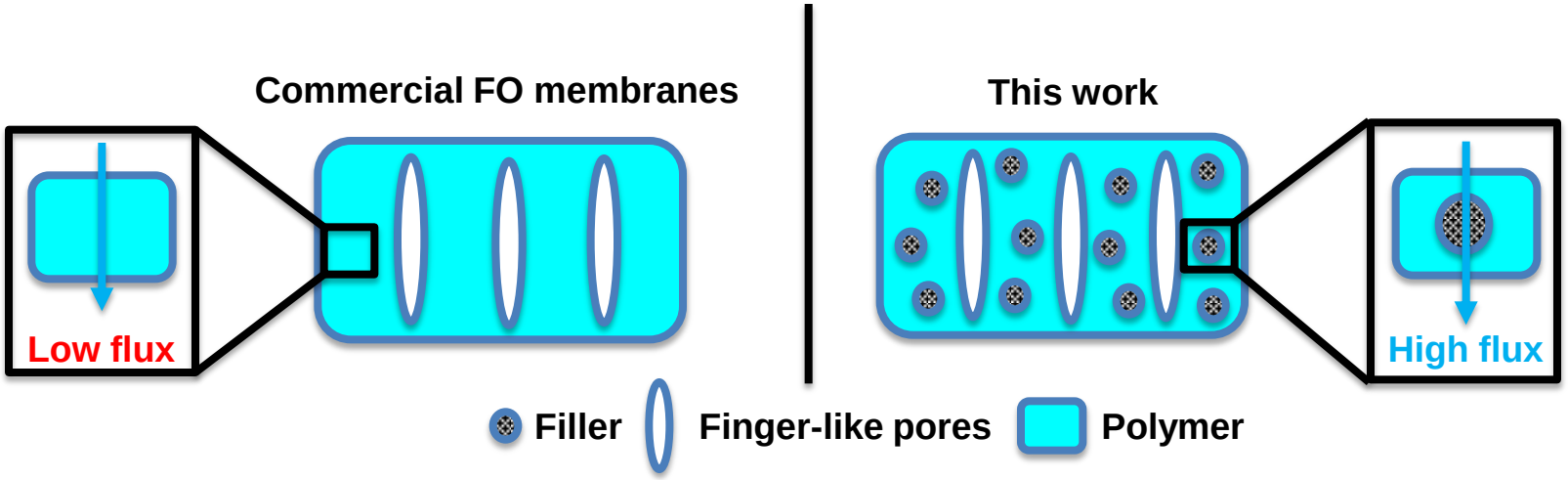
Commercial FO membranes
This work
Low flux
High flux
Filler
Finger-like pores
Polymer

# Synthesis and Characterization of Silica Gel – Polyacrylonitrile Mixed Matrix Forward Osmosis Membranes Based on Layer-by-Layer Assembly

Jian-Yuan Lee[a,b], Saren Qi[b,c], Xin Liu[b,c], Ye Li[b,c], Fengwei Huo[a,d*], Chuyang Y. Tang[e,a,b,c*]

[a] Nanyang Environment & Water Research Institute, Interdisciplinary Graduate School, Nanyang Technological University, Singapore, 639798

[c]Singapore Membrane Technology Centre, Nanyang Environment & Water Research Institute, Nanyang Technological University, Singapore, 637141

[b]School of Civil & Environmental Engineering, Nanyang Technological University, Singapore, 639798

[d]School of Materials Science and Engineering, Nanyang Technological University, Singapore, 639798

[e]Department of Civil Engineering, the University of Hong Kong, Pokfulam, Hong Kong

* Corresponding author address: Nanyang Technological University; N1-1B-35, 50 Nanyang Avenue; Singapore, 639798; Tel: (65) 6790 5267; Fax: (65) 6791 0676;

E-mail: cytang@ntu.edu.sg

E-mail: fwhuo@ntu.edu.sg

## ABSTRACT

Silica gel (SG) – polyacrylonitrile (PAN) composite Forward Osmosis (FO) membranes have been synthesized and characterized in the present work. The incorporation of SG particles into the PAN support layer significantly changed its water permeability and salt rejection rate. In the range of 0.25 – 1.0 wt.% SG loading, water permeability of membranes were enhanced after the embedment of SG, most likely due to the both porous nature of SG and the enhanced substrate porosity. However, a reduction in both water permeability and salt rejection was observed if further increase in SG loading (2.0 wt.%), possibly as a result of the agglomeration of SG. The most permeable SG-PAN FO membrane (M1.00, with 1.0 wt.% SG loading) had a significantly higher water permeability compared to the control pure PAN FO membrane (M0.00). This membrane achieved high FO water fluxes of > 100 L/m$^2$h was achieved by using the 1 M $MgCl_2$ as the draw solution (DS) and 0-10 mM NaCl as the feed solution (FS). To the best knowledge of the authors, this is the first study reporting the development and application of SG-PAN mixed matrix FO membranes (MMMs) based on layer-by-layer assembly.



**Keywords:**

silica gel (SG); mixed matrix membrane (MMM); forward osmosis (FO); phase inversion; crosslinked layer-by-layer (xLbL) assembly; internal concentration polarization.

## 1. Introduction

By using the osmotic pressure difference between a low concentration feed solution (FS) and a high concentration draw solution (DS) as the driving force to move water through a semi-permeable membrane, forward Osmosis (FO) can potentially reduce the energy consumption of current technologies by up to thirty percent [1, 2]. Compared to high pressure-driven reverse osmosis (RO) and nanofiltration (NF) membrane processes, FO process has been reported to have several advantages including (1) low energy consumption and higher fouling resistance, (2) high rejection of a variety of solutes, and (3) low operating cost because of the utilization of high osmotic pressure difference instead of the high pressure difference across the membranes as the driving force [3-5]. Hence, FO process has been employed in a wide range of applications such as wastewater treatment [4, 6-8], seawater desalination [5, 9, 10], food processing [11, 12], and valuable product concentration [12, 13].

Comprehensive reviews of FO technology have been provided by Cath et al. [1], Zhao et al. [2], and Chung et al. [14]. Existing commercial FO membranes are based on triacetate (CTA) chemistry [15]. These membranes have relatively low water permeability and are prone to hydrolysis and biodegradation. Therefore, one of the highest priorities in the research area of FO is to develop high performance FO membranes [15-26]. Generally, FO membranes are synthesized by phase inversion method [27, 28] followed by either interfacial polymerization [15, 17, 19, 23, 24, 26] or layer-by-layer (LbL) [20-22, 25], with a dense rejection layer on top of a porous support layer. One of the major limitations for these asymmetric composite FO

membranes is the internal concentration polarization (ICP), a specific and serious problem in FO process [1, 29-32]. In reality, the actual effective osmotic concentration difference will be significantly lower than the theoretical bulk osmotic concentration difference across the rejection layer [31]. Concentrative ICP occurred when the active layer faces the draw solution (AL-DS), the solutes were concentrated in the membrane porous substrate. Alternatively, dilutive ICP occurred when the active layers faces the feed solution (AL-FS), the draw solution was diluted in the support layer. In general, a smaller structural parameter *S*, which means thinner membrane, smaller tortuosity, and higher porosity of membrane) can reduce the severity of ICP during the FO process.

Recently, mixed matrix membrane (MMM) is an emerging topic under membrane development area. Several membrane properties, such as permeability, selectivity, thermal and mechanical stability, can be potentially enhanced by incorporating nanomaterials such as zeolite [33-38], silica nanoparticle [39-41], titanium oxide nanoparticle [42], and silver nanoparticle [43-45]. For example, silica nanoparticle, which has a variety of advantages such as high thermal and chemical stability, inexpensive and commercially viable, tunable particle and pore size [46, 47], has been reported to increase gas permeability without significantly decrease the selectivity of mixed matrix membranes [48-50]. The performance enhancement was believed due to the good compatibility between the polymer and the silica nanoparticle and they could be potentially used to fabricate not only gas separation, but also ultrafiltration and reverse osmosis MMM for industrial application. Unlike pressure driven membranes, FO water flux is strongly affected by ICP. The mixed matrix approach can be potentially effective in enhancing the mass transfer efficiency of membrane substrate and thus in controlling ICP. Nevertheless, the utilization of

82 silica gel (SG) as the filler for the preparation of mixed matrix FO membranes has not been
83 reported in the open literature.

84

85 The objective of current study is to improve FO performance by using SG-based mixed matrix
86 substrate. SG was embedded into polyacrylonitrile (PAN) to cast MMMs with various SG
87 loadings. The morphology, structure and performance of these SG-PAN MMMs were
88 systematically characterized. To the best knowledge of all the authors, this is the first report
89 systematically studying the synthesis and characterization of SG-PAN MMM based membranes
90 for FO application based on layer-by-layer assembly.

91

## 2. Experimental

### *2.1. Materials and chemicals*

All chemicals and reagents were used as received unless otherwise stated. PAN (Sigma–Aldrich, Mw ~150,000, Lot# MKBD6325V) was used for polymer dope solution preparation. PAN is used in the current study for its ease of processing, good chemical resistance, mechanical strength, and thermal stability [22, 51]. *N*,*N*-dimethylformamide (DMF, purity ≥99.8%, Merck) was used as solvent while lithium chloride (anhydrous LiCl, Merck) was added as the pore former, respectively. Sodium hydroxide (anhydrous NaOH, purity ≥98%, Merck) was used to prepare alkali solution for base treatment of PAN substrate to enhance hydrophilicity. Silica gel (SiliaFlash® Irregular Silica Gels - F60 Silica, SiliCycle, Lot# 070612) were used for MMMs preparation due to its high surface area, neutral pH, low trace metal content, tight particle size distribution, and well characterized properties [52]. According to the product characteristics provided by the company, the particle size and pore size of silica gel ranged from 40 to 63 μm and 55 to 65 Å respectively.

Poly(allylamine hydrochloride) (PAH, *Mw* ~ 112,000 - 200,000, Polyscience, Lot# 639458) was used as polycation and poly(sodium 4-styrene-sulfonate) (PSS, *Mw*~70,000, 30 wt.% in $H_2O$, Sigma–Aldrich, Batch# 09622HH) was used as polyanion for LbL self-assembly. The ionic strength of both PAH and PSS was adjusted by sodium chloride (NaCl, 99%, Merck). The LbL rejection layers were crosslinked by using glutaraldehyde (GA, 25% in water, Sigma–Aldrich). Previous studies [20-22, 53] have shown that xLbL FO membranes have relatively high FO water flux and good rejection to divalent ions and may have potential applications in biomass concentration, food processing, etc.

115

116 *2.2. Fabrication of PAN nanocomposite substrates*

117 To achieve good dispersion of the particles, different amounts (0.0 wt.%, 0.25 wt.%, 0.5 wt.%,
118 1.0 wt.% and 2.0 wt.% based on the dope solution) of dry silica gel particles were added into
119 DMF followed by ultrasonicated the solution for 1 h. PAN (18 wt.%) and LiCl (2 wt.%) were
120 then added into the DMF solution followed by stirring for at least 24 h at 60 $^{o}$C until a
121 homogeneous solution was obtained. The polymer solution was then cooled down to room
122 temperature overnight without stirring to completely remove any gas bubbles. A casting knife
123 was set at a gate height of 150 μm (Elcometer Pte. Ltd., Asia) was used to cast the polymer
124 solution onto a clean glass plate. The polymer film was then solidified in the tap water bath at
125 room temperature. The PAN substrate was then immersed into the 1.5 M NaOH solution at 45 $^{\circ}$C
126 for 1.5 h to partially hydrolyze the PAN substrate surface.

127

128 *2.3. Layer by layer assembly and crosslinking*

129 The details procedure for LbL rejection layer preparation can be found elsewhere [20-22, 25].
130 Briefly, the rejection layer was formed by alternatively soaking the PAN substrate into the PAH
131 and PSS solution for 15 min followed by soaking the substrate into the DI water after each
132 polyelectrolyte soaking step. Based on the optimization performed in our prior studies [21, 22],
133 the PAH/PSS treatment was repeated three times to prepare membranes rejection layer with
134 suitable rejection properties for FO applications. LbL FO membranes were cross-linked by
135 soaking the membranes in a 0.1 wt.% GA solution for 30 min followed by soaking with DI water
136 for 5 min to remove excess GA and the resulting membrane was designated as (M0.00, M0.25,

M0.50,M1.00, and M2.00). Table 1 shows the compositions of polymer dope solution and active layer.

*2.4. Membrane characterization*

The surface and cross section morphological structures of the prepared PAN membranes were characterized by field emission scanning electron microscope (FESEM, JSM-7600F, USA) [25]. A freeze-dryer was used to dry all the membranes samples at room temperature for at least 12 h followed by coated with a uniform platinum layer before observation. Element mapping was detected with the FESEM microscope equipped with energy-dispersive X-ray spectroscopy (EDX) [37]. The surface roughness of the membrane samples were tested by atomic force microscope (AFM, Park Systems XE-100, Korea). Micromeritics ASAP 2020 instrument (USA) was used to obtain the nitrogen sorption isotherm at – 196 ˚C [39]. The sample was degassed in a vacuum oven for 6 h at 200 ˚C to remove the gases and vapors absorbed on the sample surface before the measurement. By ploting the volume of nitrogen adsorption against the relative pressure, the specific surface area, pore diameter, and pore volume of silica gel was calculated using multiple point Brunauer-Emmett-Teller (BET) equation.

$$\frac{1}{\left[V_a\left(\frac{P_0}{P}-1\right)\right]}=\frac{C-1}{V_m C}\times\frac{P}{P_0}+\frac{1}{V_m C}$$

where $V_a$ is volume of gas absorbed at standard temperature and pressure and $V_m$ is volume of gas absorbed at standard temperature and pressure to produce an apparent monolayer on the sample surface. $P$ is partial vapor pressure of adsorbed gas in equilibrium with the surface at

77.4K and $P_0$ is saturated pressure of absorbed gas. $C$ is dimensionless constant that is related to the enthalpy of adsorption of the adsorbed gas on the powder sample.

By measuring the dry mass ($m_{dry}$) and wet mass ($m_{wet}$) of membrane samples, the membrane porosity ($\varepsilon$) can be calculated according to following equation [15, 54]:

$$\varepsilon = \frac{(m_{wet} - m_{dry})/\rho_w}{(m_{wet} - m_{dry})/\rho_w + m_{dry}/\rho_m} \times 100\%$$

Where $\rho_w$ and $\rho_m$ are the density of water (1.0 g/cm$^3$) and the density of PAN (1.18 g/cm$^3$). It was assumed that all the pores in the membrane and silica gel were completely filled with water. Attenuated total reflection-Fourier transform infrared spectra (ATR-FTIR, Shimadzu Prestige-21, Japan) was used to confirm the functional group on the membranes. OCA contact angle goniometer system (DataPhysics Instruments GmbH, Germany) was used to measure contact angles of the membranes and the measurement was repeated 8 times on 3 different membrane samples with the elimination of the highest and lowest two values before averaging and calculating the standard deviation. The methods for determining intrinsic separation properties such as pure water permeability, salt rejection, and salt permeability can be found elsewhere [15, 29]. Briefly, all the membranes were tested in a pressurized cross flow filtration setup using an applied pressure of 5 bars and the feed water temperature remained at 20 °C by a circulating cooling system. The effective membrane area was 42 cm$^2$. A relatively high cross flow velocity of 20 cm/s and diamond-shaped feed spacers were used to reduce the concentration polarization of feed solutes. By measuring the amount of permeate, the water permeability coefficient $A$ of membranes was determined. The $MgCl_2$ rejection $R$ were determined by conductivity

measurements (Ultra Meter II$^{TM}$ 4P, Myron L Company, CA) with the difference between the feed water and permeate water. The reported values of *A* and *R* are the average value of at least three replicates and the solute permeability coefficient *B* was calculated from the rejection and the permeate flux.

### *2.5 FO performance evaluation*

All the details of FO performance evaluation has been reported in our previous studies [37]. Briefly, a small piece of membrane with the effective membrane area of 60 $cm^2$ was used in each FO test. Both the FS and DS were pumped by two independent variable speed pump at a fixed cross flow rate of 20 cm/s on both sides of the membrane. Concentrated $MgCl_2$ solutions (0.1, 0.3, 0.5, 1.0, 2.0 or 3.0 M) were used as draw solution and the feed solution was either 10 or 100 mM NaCl solution and DI water. $MgCl_2$ was selected as the draw solute as it has high water solubility (which helps to generate a wide range of osmotic pressure), high diffusion coefficient (which helps to reduce internal concentration polarization), and good rejection by the active layers (which helps to reduce reverse solute diffusion) [2, 55]. By measuring the weight change of the FS tank with a weighing balance at fixed time intervals, the FO water flux was determined using computer data logging system. The solute flux through the FO membrane was measured by monitoring the conductivity of the FS. For each membrane sample, both the active-layer-facing-DS (AL-DS) and active-layer-facing-FS (AL-FS) orientations were tested.

The structural parameter *S* of the FO membranes was determined by [22]:

$$S = \frac{D}{J_v}\left\{\frac{C_{draw} - J_v/(A\cdot\beta R_g T) + J_s/J_v}{C_{feed} + J_s/J_v}\right\} \quad \text{(AL-DS orientation)}$$

$$S = \frac{D}{J_v}\left\{\frac{C_{draw} + J_s/J_v}{C_{feed} + J_v/(A\cdot\beta R_g T) + J_s/J_v}\right\} \quad \text{(AL-FS orientation)}$$

where $D$ is the solute diffusion coefficient; $S$ is the structural parameter of the support layer; $C_{draw}$ and $C_{feed}$ are the concentrations of draw solution and feed solution, $J_s$ is the solute flux; $\beta$ is the van't Hoff coefficient; $R_g$ is the universal gas constant; $T$ is the absolute temperature.

## 3. Results and discussion

### *3.1. Characterization of silica gel particles*

The FESEM image and the nitrogen adsorption and desorption isotherms showed that the SG particles are monodispersed microparticles with a narrow particle size of ca. 60 μm and there are relatively ordered nanopore channel (6 nm) in the particle (Fig. 1). The specific surface area for SG is 542 $m^2/g$ calculated by using the Brunauer-Emmett-Teller (BET) method.

### *3.2. Characterization of physical and chemical properties of SG-PAN MMMs*

#### *3.2.1. Morphology, thickness and porosity of SG-PAN MMMs*

Both top view and cross section images of pure PAN substrate (M0.00) and SG-PAN MMM substrates (M1.00) were shown in Fig. 2 (a) to (d). Basically, no major difference was observed on the top substrate surface. The cross-sectional images (Fig. 2 (c) and (d)) showed that less pores was observed without the SG particle (M0.00) while more straight finger-like pores were observed with SG particles (M1.00). From Fig. 2 (e) and (f), the presence of SG was observed using FESEM and further confirmed by both EDX and FTIR analysis (Fig. 3). One potential explanation is that the hydrophilic SG might facilitate the formation of pores due to decreased interfacial energy between solvent (DMF) and water during phase inversion separation [39]. As a result, a highly porous substrate (porosity of >70% based on gravimetric measurement) was obtained (Table 2). Substrate with high porosity and low tortuosity are generally favored in FO application to minimize structural parameter *S* [15]. The overall thickness of membrane substrate was ~55 μm, which is comparable to the thickness of commercial HTI FO membranes (40 – 90 μm) but is significantly thinner than that of conventional TFC RO membranes (150 μm) [22].

According to previous study, the thin cross-section, high porosity and straight pore can reduce the structural parameter of the FO membranes and thus to minimize their ICP [15, 26]. In the current study, the optimal SG-PAN MMMs (M1.00) had a relatively low *S* value (0.25 mm, compared to 0.36 mm for the pure PAN membrane M0.00).

### *3.2.2. ATR-FTIR spectra of SG-PAN MMMs*

Fig. 3 showed the ATR-FTIR spectra of the pure PAN membrane (M0.00) and the SG-PAN MMMs (M2.00). The FTIR spectra of PAN and NaOH-treated PAN have been reported in Qiu et al. [21] and Phuoc et al. [52]. For both of the membranes, the absorption peaks at 1560, which correspond to the -COONa stretching. The presence of the $-SO_3$ group of the PSS polyelectrolyte at 1006, 1035, and 1126 $cm^{-1}$ and -CH=N- group of the PAH polyelectrolyte at 1627 $cm^{-1}$ indicated that the xLbL film was successfully deposited onto the SG-PAN MMMs. Furthermore, a new peak at ~1050 $cm^{-1}$, which is attributed to the Si-OH stretching, indicates that the SG particles were successfully incorporated in the PAN membranes [39]. Its low peak intensity was likely due to the relatively low loading of silica (2 wt.%).

### *3.2.3. FESEM and AFM characterization of SG-PAN MMMs*

Top view of both FESEM and AFM of SG-PAN MMMs after xLbL synthesis is shown in Fig. 4. Generally, as the loading of silica gel in the polymer dope solution increase, surface roughness of the SG-MMMs increased. As the loading of silica gel in the polymer dope solution increase, the AFM root-mean-square (RMS) roughness, which is an indication of the mean roughness height, was significantly increased from 15 nm (M0.00) to 36 nm (M1.00), which showed greater nodular appearance on the surface of SG-MMMs. This might be due to the presence of SG cause the variation of surface roughness of SG-PAN MMMs under different loading. In general, as the surface roughness increase, the water permeability of the membrane also increases. The exact mechanism is not clear and further research is needed to explain this phenomena. In addition, the increased surface roughness may potentially affect the fouling propensity of the membrane [56,

57]. There is no much difference between PAN and SG-PAN MMMs in term of hydrophilicity and all of the membranes are quite hydrophilic with the contact angle of about $30^{o}$.

*3.3. Effect of SG loadings on intrinsic separation properties of SG-PAN MMMs*

The effect of SG loadings on intrinsic membrane separation properties, such as water permeability and salt rejection of SG-PAN MMMs, were measured by using pressurized cross flow filtration test (Appendix A). The relationship between SG loading and water permeability of the SG-PAN MMM was shown in Fig. 5. The water permeability of pure PAN substrate is 14.9 $L/m^2$ h bar. With the increment of in SG loading, the SG-PAN MMM substrate showed higher water permeability and an optimal of 24.5 $L/m^2$ h bar was attained for M1.00, which can be partially attributed to the nanoporous nature of the SG particles (Fig. 1). In addition, the SG particles may affect the phase inversion process to facilitate the formation of finger-like pore structure of the membranes due to the hydrophilic surface of SG [39]. Further increasing SG loading to 2.0 wt.% had negative impacts on the SG-PAN MMM permeability, eg. 12.5 $L/m^2$ h bar for M2.00. This might be explained by increased risk of particle agglomeration at excessive SG loading, which lead to less effective water transport in the substrate [39, 58].

As shown in Fig 5(b), the SG-PAN MMMs showed same trend to that the water permeability of the substrate. The water permeability of M0.00 is 1.85 $L/m^2$ h bar. With the increment of in SG loading, the SG-PAN MMMs showed higher water permeability and an optimal of 3.79 $L/m^2$ h bar was attained for M1.00. Further increasing SG loading to 2.0 wt.% had negative impacts on the SG-PAN MMM permeability, eg. 2.26 $L/m^2$ h bar for M2.00. The current study showed reduced $MgCl_2$ rejection at increased SG loading, which might be due to the formation of a less tight rejection layer. The salt rejection decreased from initial 91% for M0.00 to 66% for M2.00, which resulted in a drastic increase of B value from $2.6 \times 10^{-7}$ m/s to $16.6 \times 10^{-7}$ m/s. The ratio of solute permeability to water permeability ($B/A$ ratio) increased as the loadings of silica gel

increased (Appendix B). Further study is needed to optimize the membrane B\A parameter in order to reduce solute reverse diffusion and to achieve a more stable FO process [1, 2].

### *3.4. FO performance*

#### *3.4.1. Effect of SG loadings on FO performance of SG-PAN MMMs*

Fig. 6 demonstrates different SG loadings on FO performance of SG-PAN MMMs. By using 0.5 M $MgCl_2$ as DS and DI water as FS, the FO water flux is tested for both AL-DS and AL-FS orientation. Without SG loading, the xLbL membrane (M0.00) had an FO water flux of 40.8 $L/m^2$ h in AL-DS and 17.5 $L/m^2$ h in AL-FS. The much lower flux in AL-FS can be attributed to the dilution of draw solution in the membrane substrate in this orientation [29, 31]. The embedment of SG particles increased the FO water flux initially for a SG loading up to 1.0 wt.% and further increase SG loading caused the water flux reduction. This might be explained by increased risk of particle agglomeration at excessive SG loading, which lead to less effective water transport in the substrate [39, 58]. In addition, this result is consistent with the water permeability *A* of SG-PAN MMMs, where the membrane with the optimal water permeability also had the optimal FO water flux (M1.00). For the AL-FS orientation, the same trend was also observed, where once again the SG-PAN membrane (M1.00) showed the highest water flux. With a 0.5 M $MgCl_2$ as the DS and DI water as the FS, M1.00 had water flux of 77.9 $L/m^2$ h in AL-DS and 28.6 $L/m^2$ h in AL-FS. The water flux of the pure PAN membrane (M0.00) were significantly lower than these values, suggesting that the incorporation of SG particles as an effective approach for enhanced FO water flux performance.

306 The *Js/Jv* ratio of SG-MMMs is shown in Fig. 6(b) for both the AL-DS and AL-FS orientation.
307 The term *Js/Jv* ratio represents the effective solute concentration reverse diffused through an FO
308 membrane. When evaluating FO membranes, we need to consider both water flux and solute flux
309 at the same time. Previous studies have revealed that lower *Js/Jv* value is preferred to avoid
310 excessive fouling and solute accumulation in FO processes, less severe membrane fouling as
311 well as decreased the replenishment cost where DS regeneration is needed [20-22, 25]. We
312 observed for the SG-PAN MMMs that (1) a very small value of *Js/Jv* ratio was obtained (<0.3
313 g/L), (2) *Js/Jv* ratio was slightly higher in AL-FS compared to AL-DS, and (3) *Js/Jv* ratio remain
314 nearly constant for a SG loading up to 1.0 wt.% and further increase SG loading resulted in
315 slightly higher *Js/Jv* ratio in both AL-DS and AL-FS. The SG-PAN MMM membrane (M2.00)
316 has the highest *Js/Jv* ratio in both AL-DS and AL-FS. The high *Js/Jv* value can be contributed to
317 the low solute rejection by the membrane and the corresponding high *B/A* value. With a 0.5 M
318 $MgCl_2$ DS and DI water FS, M2.00 had *Js/Jv* ratio of 0.12 g/L in AL-DS and 0.25 g/L in AL-FS.
319 The *Js/Jv* ratio of the pure PAN membrane (M0.00) was slightly lower than these values,
320 suggesting that the incorporation of excess SG particles decreased the selectivity of SG-PAN
321 MMMs. Therefore, it is very crucial to optimize the SG loading because of excess SG particles
322 (eg. from 1 wt.% to 2.wt.% in this study) may dramatically increase the solute flux and decrease
323 the water flux at the same time (ie. the *Js/Jv* ratio increased). Comparison of FO performance of
324 the SG-PAN MMM membranes with other FO membranes in literature was shown in Table 3.

325

326 *3.4.2. Effect of draw solution and feed solution concentrations on FO performance of SG-PAN*
327 *MMMs*

The FO water performance of SG-PAN MMMs (M1.00) is presented in Fig. 7 for a variety of DS concentrations (0.1, 0.3, 0.5, 1.0, 2.0, 3.0 M $MgCl_2$) and FS concentrations (0, 10, 100 mM NaCl). Regardless of the membrane orientation, higher the concentration of the DS resulted in higher the FO water flux for the SG-PAN MMM due to the larger osmotic pressure as the driving force across the membrane. In AL-DS orientation, the FO water flux of SG-PAN MMM (M1.00) was 20 $L/m^2$ h for a 0.1 M $MgCl_2$ and it increased to 77.9 $L/m^2$ h at 0.5 M $MgCl_2$ as a result of increased the osmotic driving force. The highest FO water flux of 121 $L/m^2$ h was achieved by using the 2.0 M $MgCl_2$ as the DS and DI water as the FS, this clearly demonstrates the potential of SG-PAN MMMs for high flux FO application. However, further increase the concentration of DS to 3.0 M $MgCl_2$ did not result in additional gain in water flux. This is consistent with prior studies [10, 59] that ICP increases and FO efficiency decreases at higher DS concentrations.

The FO water performance of SG-PAN MMMs (M1.00) is presented in Fig. 7(b) for various FS concentrations using 1.0 M $MgCl_2$ DS. Regardless of the membrane orientation, higher FS concentration decreased the osmotic pressure driving force across the membrane and hence decreased the water flux of the SG-PAN MMMs. With a 1.0 M $MgCl_2$ as the DS and DI water as the FS, M1.00 had water flux of 117 $L/m^2$ h in AL-DS and 41 $L/m^2$ h in AL-FS. These values were significantly higher than those of the commercial HTI Hydrowell membranes, which had water flux of 36.3 $L/m^2$ h in AL-DS and 15.8 $L/m^2$ h in AL-FS, under the same testing condition. However, further increasing the FS concentration from 10 mM to 100 mM NaCl solution, the FO water flux decreased sharply from 106 $L/m^2$ h to 65.4 $L/m^2$ h in AL-DS orientation and the FO water flux decreased slightly from 37.4 $L/m^2$ h to 33.8 $L/m^2$ h in AL-FS orientation.

## 4. Conclusions

In summary, SG-PAN MMM based FO membranes with and without SG particles were systematically synthesized and characterized in this study. SG-PAN MMMs can significantly enhance FO water flux probably due to both the nanometer pores in the SG particles and enhanced substrate porosity upon embedment into the membrane substrate layer. Both the intrinsic separation properties and surface chemistry and of SG-PAN MMMs were enhanced by various SG loadings. The highest FO water flux of 121 $L/m^2 h$ was achieved by using the 2.0 M $MgCl_2$ as the DS and DI water as the FS. The current study demonstrates the potential of use of MMMs for improving the substrate porosity and mass transfer coefficient as well as the rejection layer properties. This opens an additional dimension for ICP control in osmotically-driven membrane processes.

## Acknowledgment

The authors thank the Singapore Ministry of Education (Grant #MOE2011-T2-2-035, ARC 3/12) for the financial support of the work. We also thank the Campus for Research Excellence and Technological Enterprise (CREATE) programme Nanomaterials for Energy and Water Management under the funding of Singapore National Research Foundation.

## Reference


[1] T.Y. Cath, A.E. Childress, M. Elimelech, Forward osmosis: Principles, applications, and recent developments, Journal of Membrane Science, 281 (2006) 70-87.

[2] S.F. Zhao, L. Zou, C.Y.Y. Tang, D. Mulcahy, Recent developments in forward osmosis: Opportunities and challenges, Journal of Membrane Science, 396 (2012) 1-21.

[3] S. Lee, C. Boo, M. Elimelech, S. Hong, Comparison of fouling behavior in forward osmosis (FO) and reverse osmosis (RO), Journal of Membrane Science, 365 (2010) 34-39.

[4] A. Achilli, T.Y. Cath, E.A. Marchand, A.E. Childress, The forward osmosis membrane bioreactor: A low fouling alternative to MBR processes, Desalination, 239 (2009) 10-21.

[5] J.R. McCutcheon, R.L. McGinnis, M. Elimelech, A novel ammonia-carbon dioxide forward (direct) osmosis desalination process, Desalination, 174 (2005) 1-11.

[6] R.W. Holloway, A.E. Childress, K.E. Dennett, T.Y. Cath, Forward osmosis for concentration of anaerobic digester centrate, Water Research, 41 (2007) 4005-4014.

[7] E.R. Cornelissen, D. Harmsen, K.F. de Korte, C.J. Ruiken, J.J. Qin, H. Oo, L.P. Wessels, Membrane fouling and process performance of forward osmosis membranes on activated sludge, Journal of Membrane Science, 319 (2008) 158-168.

[8] W.C.L. Lay, Q.Y. Zhang, J.S. Zhang, D. McDougald, C.Y. Tang, R. Wang, Y. Liu, A.G. Fane, Study of integration of forward osmosis and biological process: Membrane performance under elevated salt environment, Desalination, 283 (2011) 123-130.

[9] J.O. Kessler, C.D. Moody, Drinking water from sea water by forward osmosis, Desalination, 18 (1976) 297-306.

[10] R.L. McGinnis, M. Elimelech, Energy requirements of ammonia-carbon dioxide forward osmosis desalination, Desalination, 207 (2007) 370-382.

[11] K.B. Petrotos, P. Quantick, H. Petropakis, A study of the direct osmotic concentration of tomato juice in tubular membrane - module configuration. I. The effect of certain basic process parameters on the process performance, Journal of Membrane Science, 150 (1998) 99-110.

[12] D. Torreggiani, G. Bertolo, Present and future in process control and optimization of osmotic dehydration. From unit operation to innovative combined process: an overview, Advances in food and nutrition research, 48 (2004) 173-238.

[13] S. Zou, Y.S. Gu, D.Z. Xiao, C.Y.Y. Tang, The role of physical and chemical parameters on forward osmosis membrane fouling during algae separation, Journal of Membrane Science, 366 (2011) 356-362.

[14] T.-S. Chung, X. Li, R.C. Ong, Q. Ge, H. Wang, G. Han, Emerging forward osmosis (FO) technologies and challenges ahead for clean water and clean energy applications, Current Opinion in Chemical Engineering, 1 (2012) 246-257.

[15] J. Wei, C.Q. Qiu, C.Y.Y. Tang, R. Wang, A.G. Fane, Synthesis and characterization of flat-sheet thin film composite forward osmosis membranes, Journal of Membrane Science, 372 (2011) 292-302.

[16] J.C. Su, Q. Yang, J.F. Teo, T.S. Chung, Cellulose acetate nanofiltration hollow fiber membranes for forward osmosis processes, Journal of Membrane Science, 355 (2010) 36-44.

[17] R. Wang, L. Shi, C.Y.Y. Tang, S.R. Chou, C. Qiu, A.G. Fane, Characterization of novel forward osmosis hollow fiber membranes, Journal of Membrane Science, 355 (2010) 158-167.

[18] S.R. Chou, L. Shi, R. Wang, C.Y.Y. Tang, C.Q. Qiu, A.G. Fane, Characteristics and potential applications of a novel forward osmosis hollow fiber membrane, Desalination, 261 (2010) 365-372.

[19] S.R. Chou, R. Wang, L. Shi, Q.H. She, C.Y. Tang, A.G. Fane, Thin-film composite hollow fiber membranes for pressure retarded osmosis (PRO) process with high power density, Journal of Membrane Science, 389 (2012) 25-33.

[20] S.R. Qi, C.Q. Qiu, Y. Zhao, C.Y.Y. Tang, Double-skinned forward osmosis membranes based on layer-by-layer assembly-FO performance and fouling behavior, Journal of Membrane Science, 405 (2012) 20-29.

[21] C.Q. Qiu, S.R. Qi, C.Y.Y. Tang, Synthesis of high flux forward osmosis membranes by chemically crosslinked layer-by-layer polyelectrolytes, Journal of Membrane Science, 381 (2011) 74-80.

[22] Q. Saren, C. Qiu, C. Tang, Synthesis and Characterization of Novel Forward Osmosis Membranes based on Layer-by-Layer Assembly, Environmental Science & Technology, 45 (2011) 5201-5208.

[23] A. Tiraferri, N.Y. Yip, W.A. Phillip, J.D. Schiffman, M. Elimelech, Relating performance of thin-film composite forward osmosis membranes to support layer formation and structure, Journal of Membrane Science, 367 (2011) 340-352.

[24] N.Y. Yip, A. Tiraferri, W.A. Phillip, J.D. Schiffman, M. Elimelech, High Performance Thin-Film Composite Forward Osmosis Membrane, Environmental Science & Technology, 44 (2010) 3812-3818.

[25] S.R. Qi, W.Y. Li, Y. Zhao, N. Ma, J. Wei, T.W. Chin, C.Y.Y. Tang, Influence of the properties of layer-by-layer active layers on forward osmosis performance, Journal of Membrane Science, 423 (2012) 536-542.

[26] J. Wei, X. Liu, C.Q. Qiu, R. Wang, C.Y.Y. Tang, Influence of monomer concentrations on the performance of polyamide-based thin film composite forward osmosis membranes, Journal of Membrane Science, 381 (2011) 110-117.

[27] M. Sairam, E. Sereewatthanawut, K. Li, A. Bismarck, A.G. Livingston, Method for the preparation of cellulose acetate flat sheet composite membranes for forward osmosis-Desalination using MgSO4 draw solution, Desalination, 273 (2011) 299-307.

[28] Q. Yang, K.Y. Wang, T.S. Chung, Dual-Layer Hollow Fibers with Enhanced Flux As Novel Forward Osmosis Membranes for Water Production, Environmental Science & Technology, 43 (2009) 2800-2805.

[29] C.Y.Y. Tang, Q.H. She, W.C.L. Lay, R. Wang, A.G. Fane, Coupled effects of internal concentration polarization and fouling on flux behavior of forward osmosis membranes during humic acid filtration, Journal of Membrane Science, 354 (2010) 123-133.

[30] S. Loeb, L. Titelman, E. Korngold, J. Freiman, Effect of porous support fabric on osmosis through a Loeb-Sourirajan type asymmetric membrane, Journal of Membrane Science, 129 (1997) 243-249.

[31] J.R. McCutcheon, M. Elimelech, Influence of concentrative and dilutive internal concentration polarization on flux behavior in forward osmosis, Journal of Membrane Science, 284 (2006) 237-247.

[32] G.T. Gray, J.R. McCutcheon, M. Elimelech, Internal concentration polarization in forward osmosis: role of membrane orientation, Desalination, 197 (2006) 1-8.

[33] M. Fathizadeh, A. Aroujalian, A. Raisi, Effect of added NaX nano-zeolite into polyamide as a top thin layer of membrane on water flux and salt rejection in a reverse osmosis process, Journal of Membrane Science, 375 (2011) 88-95.

[34] B.H. Jeong, E.M.V. Hoek, Y.S. Yan, A. Subramani, X.F. Huang, G. Hurwitz, A.K. Ghosh, A. Jawor, Interfacial polymerization of thin film nanocomposites: A new concept for reverse osmosis membranes, Journal of Membrane Science, 294 (2007) 1-7.

[35] M.L. Lind, A.K. Ghosh, A. Jawor, X.F. Huang, W. Hou, Y. Yang, E.M.V. Hoek, Influence of Zeolite Crystal Size on Zeolite-Polyamide Thin Film Nanocomposite Membranes, Langmuir, 25 (2009) 10139-10145.

[36] M.L. Lind, B.H. Jeong, A. Subramani, X.F. Huang, E.M.V. Hoek, Effect of mobile cation on zeolite-polyamide thin film nanocomposite membranes, Journal of Materials Research, 24 (2009) 1624-1631.

[37] N. Ma, J. Wei, R. Liao, C.Y. Tang, Zeolite-polyamide thin film nanocomposite membranes: Towards enhanced performance for forward osmosis, Journal of Membrane Science, 405-406 (2012) 149-157.

[38] N. Ma, J. Wei, S.R. Qi, Y. Zhao, Y.B. Gao, C.Y.Y. Tang, Nanocomposite substrates for controlling internal concentration polarization in forward osmosis membranes, Journal of Membrane Science, 441 (2013) 54-62.

[39] J. Huang, K.S. Zhang, K. Wang, Z.L. Xie, B. Ladewig, H.T. Wang, Fabrication of polyethersulfone-mesoporous silica nanocomposite ultrafiltration membranes with antifouling properties, Journal of Membrane Science, 423 (2012) 362-370.

[40] G.L. Jadav, P.S. Singh, Synthesis of novel silica-polyamide nanocomposite membrane with enhanced properties, Journal of Membrane Science, 328 (2009) 257-267.

[41] H.Q. Wu, B.B. Tang, P.Y. Wu, Optimizing polyamide thin film composite membrane covalently bonded with modified mesoporous silica nanoparticles, Journal of Membrane Science, 428 (2013) 341-348.

[42] H.S. Lee, S.J. Im, J.H. Kim, H.J. Kim, J.P. Kim, B.R. Min, Polyamide thin-film nanofiltration membranes containing TiO2 nanoparticles, Desalination, 219 (2008) 48-56.

[43] E.S. Kim, G. Hwang, M.G. El-Din, Y. Liu, Development of nanosilver and multi-walled carbon nanotubes thin-film nanocomposite membrane for enhanced water treatment, Journal of Membrane Science, 394 (2012) 37-48.

[44] S.Y. Lee, H.J. Kim, R. Patel, S.J. Im, J.H. Kim, B.R. Min, Silver nanoparticles immobilized on thin film composite polyamide membrane: characterization, nanofiltration, antifouling properties, Polymers for Advanced Technologies, 18 (2007) 562-568.

[45] X. Liu, S. Qi, Y. Li, L. Yang, B. Cao, C.Y. Tang, Synthesis and characterization of novel antibacterial silver nanocomposite nanofiltration and forward osmosis membranes based on layer-by-layer assembly, Water Research, 47 (2013) 3081-3092.

[46] C.C. Liu, X.M. Wang, S. Lee, L.D. Pfefferle, G.L. Haller, Surfactant chain length effect on the hexagonal-to-cubic phase transition in mesoporous silica synthesis, Microporous and Mesoporous Materials, 147 (2012) 242-251.

[47] H.H. Dai, J.T. Yang, J.P. Ma, F. Chen, Z.D. Fei, M.Q. Zhong, A green process for the synthesis of controllable mesoporous silica materials, Microporous and Mesoporous Materials, 147 (2012) 281-285.

[48] A. Sharif, H. Koolivand, G. Khanbabaie, M. Hemmati, J. Aalaie, M.R. Kashani, A. Gheshlaghi, Improvement of CO2/CH4 separation characteristics of polyethersulfone by modifying with polydimethylsiloxane and nano-silica, Journal of Polymer Research, 19 (2012).

[49] Y. Shen, A.C. Lua, Preparation and characterization of mixed matrix membranes based on PVDF and three inorganic fillers (fumed nonporous silica, zeolite 4A and mesoporous MCM-41) for gas separation, Chemical Engineering Journal, 192 (2012) 201-210.

[50] K.S. Jang, H.J. Kim, J.R. Johnson, W.G. Kim, W.J. Koros, C.W. Jones, S. Nair, Modified Mesoporous Silica Gas Separation Membranes on Polymeric Hollow Fibers, Chemistry of Materials, 23 (2011) 3025-3028.

[51] F.-J. Fu, S. Zhang, S.-P. Sun, K.-Y. Wang, T.-S. Chung, POSS-containing Delamination-free Dual-layer Hollow Fiber Membranes for Forward Osmosis and Osmotic Power Generation, Journal of Membrane Science.

[52] http://www.silicycle.com/products/siliaflash-irregular-silica-gels/advantages-of-siliaflash-over-competitors-products.

[53] P.H.H. Duong, J. Zuo, T.S. Chung, Highly crosslinked layer-by-layer polyelectrolyte FO membranes: Understanding effects of salt concentration and deposition time on FO performance, Journal of Membrane Science, 427 (2013) 411-421.

[54] P. Sukitpaneenit, T.-S. Chung, Molecular elucidation of morphology and mechanical properties of PVDF hollow fiber membranes from aspects of phase inversion, crystallization and rheology, Journal of Membrane Science, 340 (2009) 192-205.

[55] A. Achilli, T.Y. Cath, A.E. Childress, Selection of inorganic-based draw solutions for forward osmosis applications, Journal of Membrane Science, 364 (2010) 233-241.

[56] J. Wei, C. Qiu, Y. Wang, R. Wang, C.Y. Tang, Comparison of NF-like and RO-like thin film composite osmotically-driven membranes - Implications for membrane selection and process optimization, Journal of Membrane Science, 427 (2013) 460-471.

[57] Y. Gu, Y.-N. Wang, J. Wei, C.Y. Tang, Organic fouling of thin-film composite polyamide and cellulose triacetate forward osmosis membranes by oppositely charged macromolecules, Water Research, 47 (2013) 1867-1874.

[58] J.N. Shen, H.M. Ruan, L.G. Wu, C.J. Gao, Preparation and characterization of PES-SiO2 organic-inorganic composite ultrafiltration membrane for raw water pretreatment, Chemical Engineering Journal, 168 (2011) 1272-1278.

[59] Y. Xu, X. Peng, C.Y. Tang, Q.S. Fu, S. Nie, Effect of draw solution concentration and operating conditions on forward osmosis and pressure retarded osmosis performance in a spiral wound module, Journal of Membrane Science, 348 (2010) 298-309.

## Appendix A

**Pressurized cross flow filtration setup.**

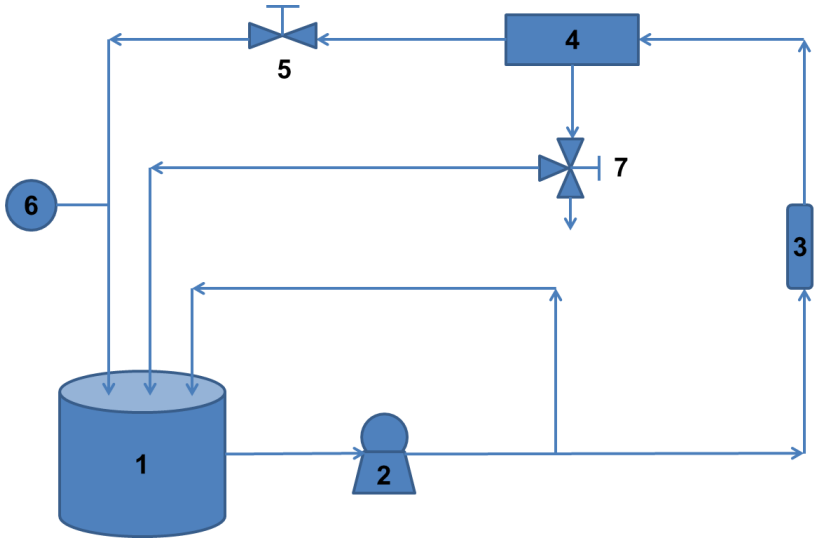


(1) Feed tank, (2) pump, (3) liquid flowmeters, (4) membrane cells, (5) regulating valves, (6) pressure gauges, (7) three-port valves. [37]

## Appendix B

**Intrinsic separation properties of SG-PAN MMM membrane with different silica gel loading[a].**

| Membrane | Water permeability after NaOH treatment[b] | Water permeability A after xLbL synthesis[b] | | $MgCl_2$ Rejection[c] (%) | Salt Permeability B[c] ($\times10^{-7}$m/s) | $B/A$[c] (kPa) |
|---|---|---|---|---|---|---|
| | ($L/m^2$ h bar) | ($L/m^2$ h bar) | ($\times10^{-12}$m/s Pa) | | | |
| M0.00 | 14.9 ± 0.4 | 1.85 ± 0.10 | 5.2 ± 0.3 | 91 | 2.6 ± 0.4 | 49.6 |
| M0.25 | 16.3 ± 0.9 | 3.50 ± 0.11 | 9.7 ± 0.3 | 84 | 9.0 ± 1.6 | 92.4 |
| M0.50 | 22.3 ± 0.4 | 3.35 ± 0.08 | 9.3 ± 0.2 | 83 | 9.6 ± 1.6 | 102 |
| M1.00 | 24.5 ± 0.9 | 3.79 ± 0.17 | 10.5 ± 0.5 | 76 | 16.9 ± 1.1 | 161 |
| M2.00 | 12.1 ± 0.7 | 2.26 ± 0.13 | 6.3 ± 0.4 | 66 | 16.6 ± 5.8 | 262 |

[a] The experiment errors are reported as the standard deviation of at least 3 repeated measurements.

[b] Measured at an applied pressure of 5 bar with ultrapure water as feed water in the pressurized cross flow filtration testing mode.

[c] Measured at an applied pressure of 5 bar with 5 mM $MgCl_2$ as feed water in the pressurized cross flow filtration testing mode.

544 **Table 1.** Flat-sheet SG-PAN MMMs with different SG loading.

| Membrane | Substrate | | | | Active Layer | |
|---|---|---|---|---|---|---|
| | PAN (wt.%) | DMF (wt.%) | LiCl (wt.%) | SG (wt.%) | PAH (g/L) | PSS (g/L) |
| M0.00 | 18 | 80.00 | 2.0 | 0.00 | 1.0 | 1.0 |
| M0.25 | 18 | 79.75 | 2.0 | 0.25 | 1.0 | 1.0 |
| M0.50 | 18 | 79.50 | 2.0 | 0.50 | 1.0 | 1.0 |
| M1.00 | 18 | 79.00 | 2.0 | 1.00 | 1.0 | 1.0 |
| M2.00 | 18 | 78.00 | 2.0 | 2.00 | 1.0 | 1.0 |

545

546

547 **Table 2.** Membrane thickness, membrane porosity, surface roughness, and contact angle of SG-
548 PAN MMMs with different loading of silica gel.

| Membrane | Membrane Thickness (μm) | Membrane Porosity ε (%) | Surface Roughness $R_a$ (nm) | Contact Angle ($^o$) | Structural Parameter (mm) |
|---|---|---|---|---|---|
| M0.00 | 56 ± 1 | 67 ± 1 | 15 ± 1 | 34 ± 2 | 0.36 ± 0.03 |
| M0.25 | 52 ± 1 | 73 ± 5 | 21 ± 2 | 28 ± 1 | 0.44 ± 0.01 |
| M0.50 | 55 ± 1 | 78 ± 4 | 33 ± 3 | 26 ± 2 | 0.28 ± 0.02 |
| M1.00 | 54 ± 1 | 79 ± 1 | 36 ± 8 | 30 ± 1 | 0.25 ± 0.01 |
| M2.00 | 59 ± 1 | 80 ± 3 | 15 ± 1 | 33 ± 1 | 0.34 ± 0.01 |

549

550 Table 3. Comparison of FO performance of the SG-PAN MMM membranes with other FO membranes in literature

| Membranes | $J_v$ ($L/m^2h$) | $J_s$ ($g/m^2h$) | $J_s/J_v$ (g/L) | FS | DS: $MgCl_2$ (M) | orientation | Temp. (°C) | Reference Number |
|---|---|---|---|---|---|---|---|---|
| M0.00 [a] | 17.5 | 2.7 | 0.15 | DI | 0.5 | AL-FS | 25 ± 1 | current study |
| | 40.8 | 3.2 | 0.08 | DI | 0.5 | AL-DS | 25 ± 1 | |
| M0.25 [a] | 19.5 | 3.5 | 0.18 | DI | 0.5 | AL-FS | 25 ± 1 | |
| | 54.7 | 3.9 | 0.07 | DI | 0.5 | AL-DS | 25 ± 1 | |
| M0.50 [a] | 25.3 | 4.8 | 0.19 | DI | 0.5 | AL-FS | 25 ± 1 | |
| | 67.3 | 5.8 | 0.09 | DI | 0.5 | AL-DS | 25 ± 1 | |
| M1.00 [a] | 28.6 | 5.8 | 0.20 | DI | 0.5 | AL-FS | 25 ± 1 | |
| | 77.9 | 6.9 | 0.09 | DI | 0.5 | AL-DS | 25 ± 1 | |
| M2.00 [a] | 19.6 | 4.8 | 0.25 | DI | 0.5 | AL-FS | 25 ± 1 | |
| | 45.7 | 5.7 | 0.12 | DI | 0.5 | AL-DS | 25 ± 1 | |
| xLbL2.5 [b] | 17.2 | 2.0 | 0.120 | 10 mM NaCl /DI | 0.5 | AL-FS | 23 ± 1 | 45 |
| | 39.3 | 3.1 | 0.071 | 10 mM NaCl /DI | 0.5 | AL-DS | 23 ± 1 | |
| xLbL3-3 [c] | 42.3 | 12.0 | 0.284 | DI | 0.5 | AL-DS | 22 ± 0.5 | 20 |
| | 35.5 | N.A. | N.A. | 10 mM NaCl | 0.5 | AL-DS | 22 ± 0.5 | |
| xLbL [d] | 30.0 [m] | 5.8 | 0.193 [m] | DI | 0.5 | AL-FS | 23 | 21 |

| | | | | | | | | |
|---|---|---|---|---|---|---|---|---|
| | 60.0 [m] | 3.5 | 0.058 [m] | DI | 0.5 | AL-DS | 23 | |
| 3#LbL FO [e] | 28.7 | 10.5 | 0.366 | DI | 1 | AL-FS | 23 ± 1 | 22 |
| | 25.3 | N.A. | N.A. | 10 mM NaCl | 1 | AL-FS | 23 ± 1 | |
| | 31.7 | 28.6 | 0.903 | DI | 1 | AL-DS | 23 ± 1 | |
| | 23.8 | N.A. | N.A. | 10 mM NaCl | 1 | AL-DS | 23 ± 1 | |
| HTI [f] | 15.8 | 1.2 | 0.074 | DI | 1 | AL-FS | 23 ± 1 | |
| | 36.3 | 7.6 | 0.209 | DI | 1 | AL-DS | 23 ± 1 | |

[a] $J_v$ values were obtained by using 0.5 M $MgCl_2$ as draw solution and DI water as feed solution.

[b] $J_v$ values were obtained by using 0.5 M $MgCl_2$ as draw solution and DI water or 10 mM Nacl as feed solution.

[c] Cross-linked double-skinned NF-like flat sheet FO membranes

[d] Cross-linked NF-like flat sheet FO membranes

[e] Flat sheet FO membranes

[f] Commercial flat sheet thin film FO membrane.

## Figures

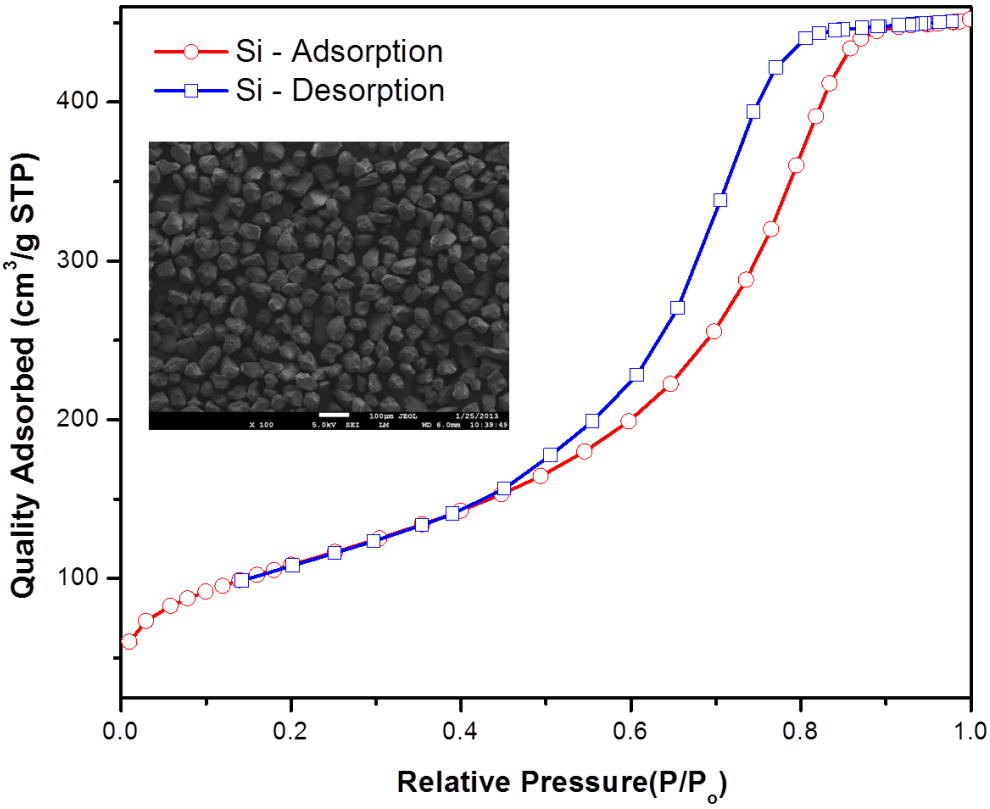


**Fig. 1.** Nitrogen sorption isotherm of silica gel and the inset is the FESEM micrographs of silica gel.

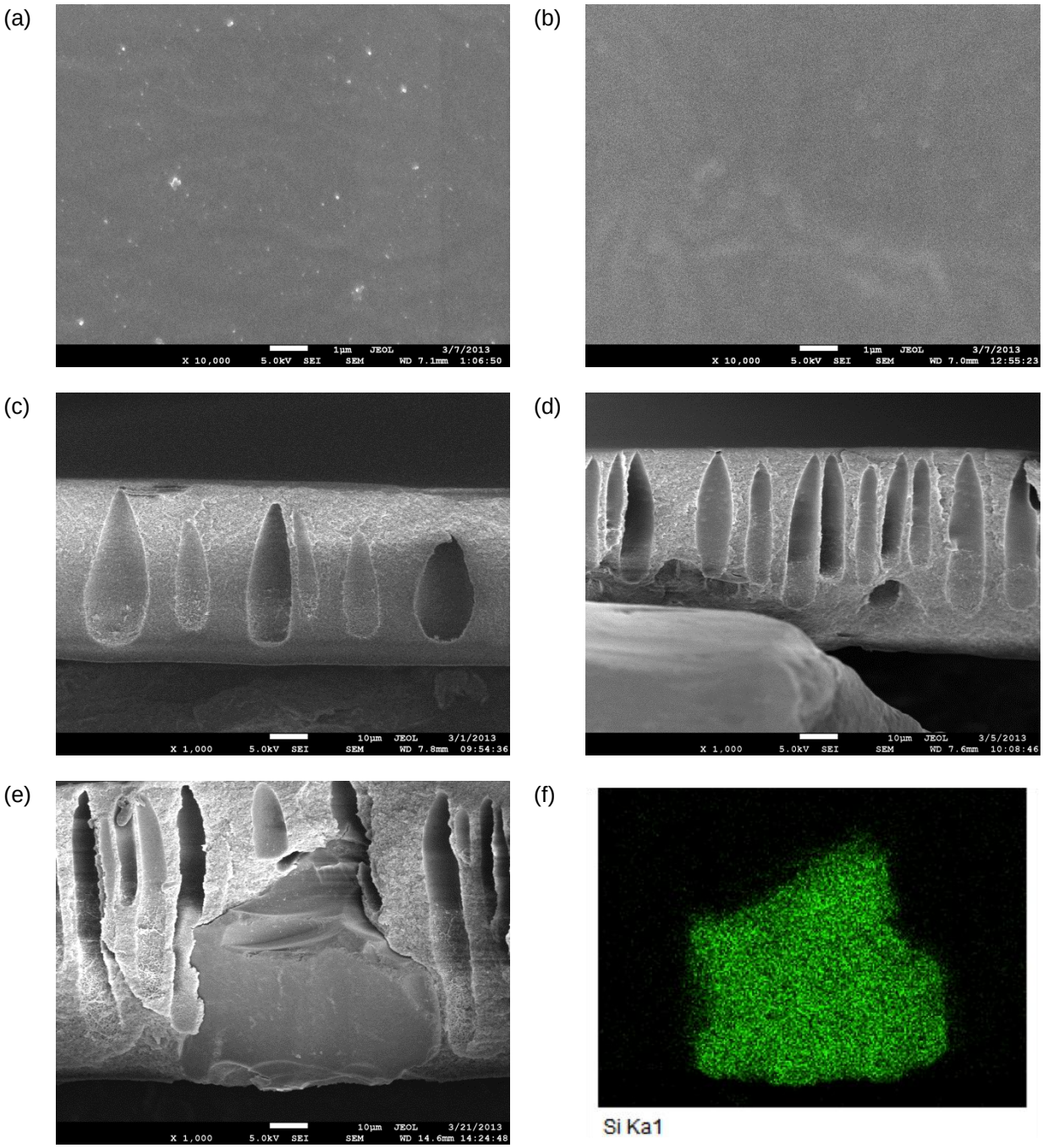


**Fig. 2.** FESEM micrographs of the membranes substrate. (a) Top surface and (c) cross-section of M0.00 substrate; (b) top surface and (d) cross-section of M1.00 substrate; (e) and (f) FESEM and EDX image of M1.00 substrate confirmed that SG particle was successfully incorporated into the membranes.

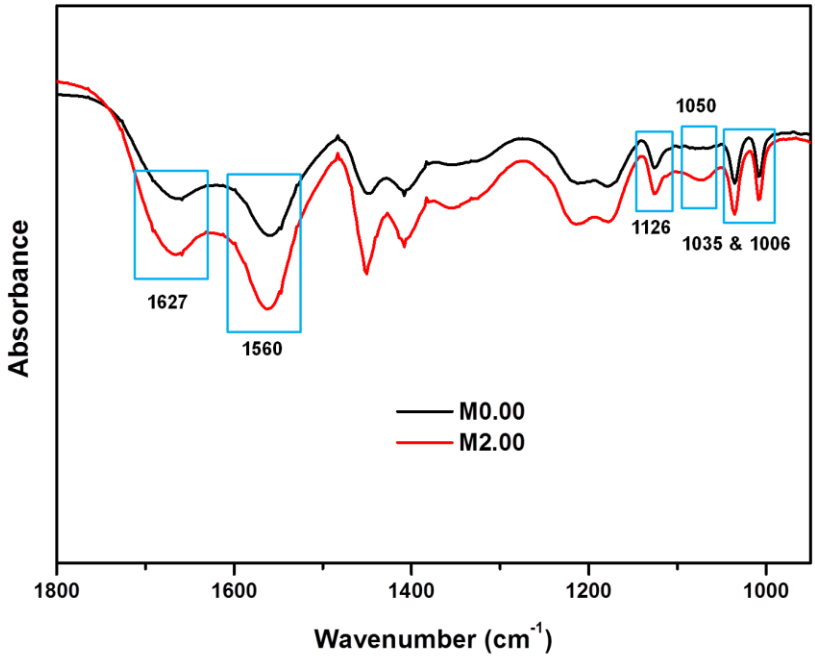


**Fig. 3.** FTIR spectra of pure PAN membranes (M0.00) and SG-PAN MMM (M2.00). A new peak at ~1050 $cm^{-1}$ was due to the Si-OH stretching of silica gel.

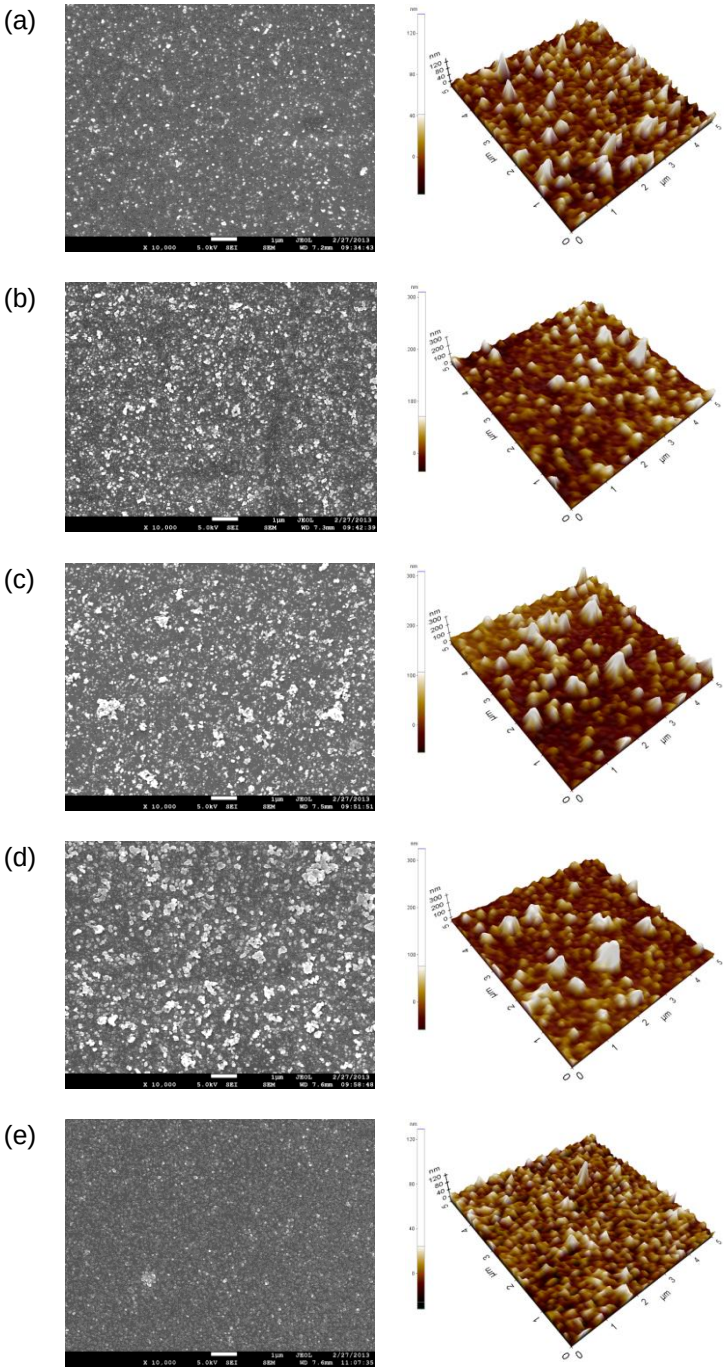


**Fig. 4.** FESEM and AFM characterization of (a) M0.00, (b) M0.25, (c) M0.50, (d) M1.00 and (e) M2.00.

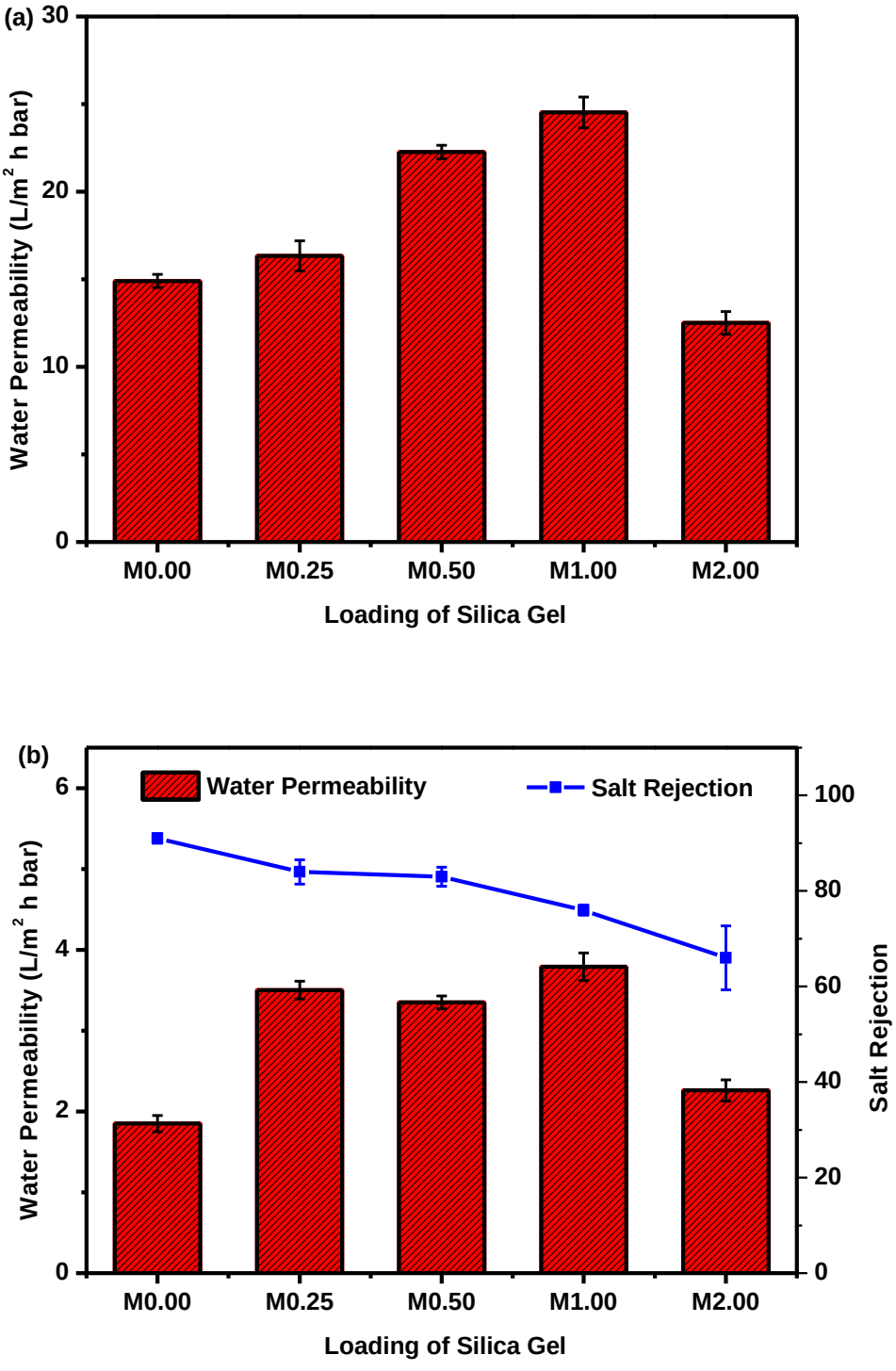


**Fig. 5.** Effect of different silica gel loading on (a) the pure water permeability of the membranes substrate after NaOH treatment and (b) on the performance of RO after xLbL synthesis. Testing conditions: DI water or 5 mM $MgCl_2$ as the feed solution; applied pressure: 5 bars, error bar was based on the standard deviation of 3 replicate measurements.

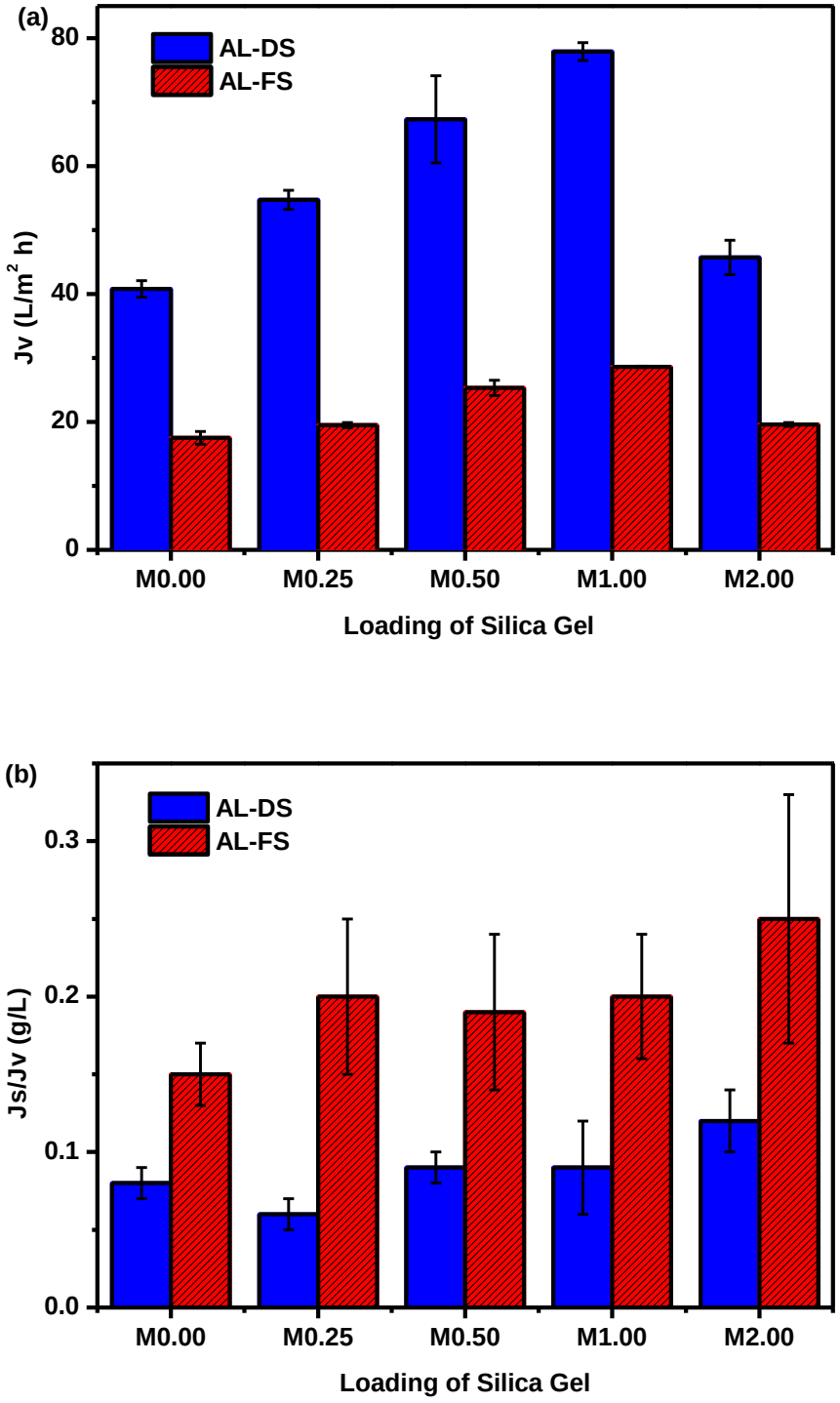


**Fig. 6.** Effect of silica gel loading on (a) FO water flux, and (b) ratio of solute flux over water flux of SG-PAN MMM membranes. Testing conditions: 0.5 M $MgCl_2$ as the draw solution and DI water as the feed solution, error bar was based on the standard deviation of 3 replicate measurements.

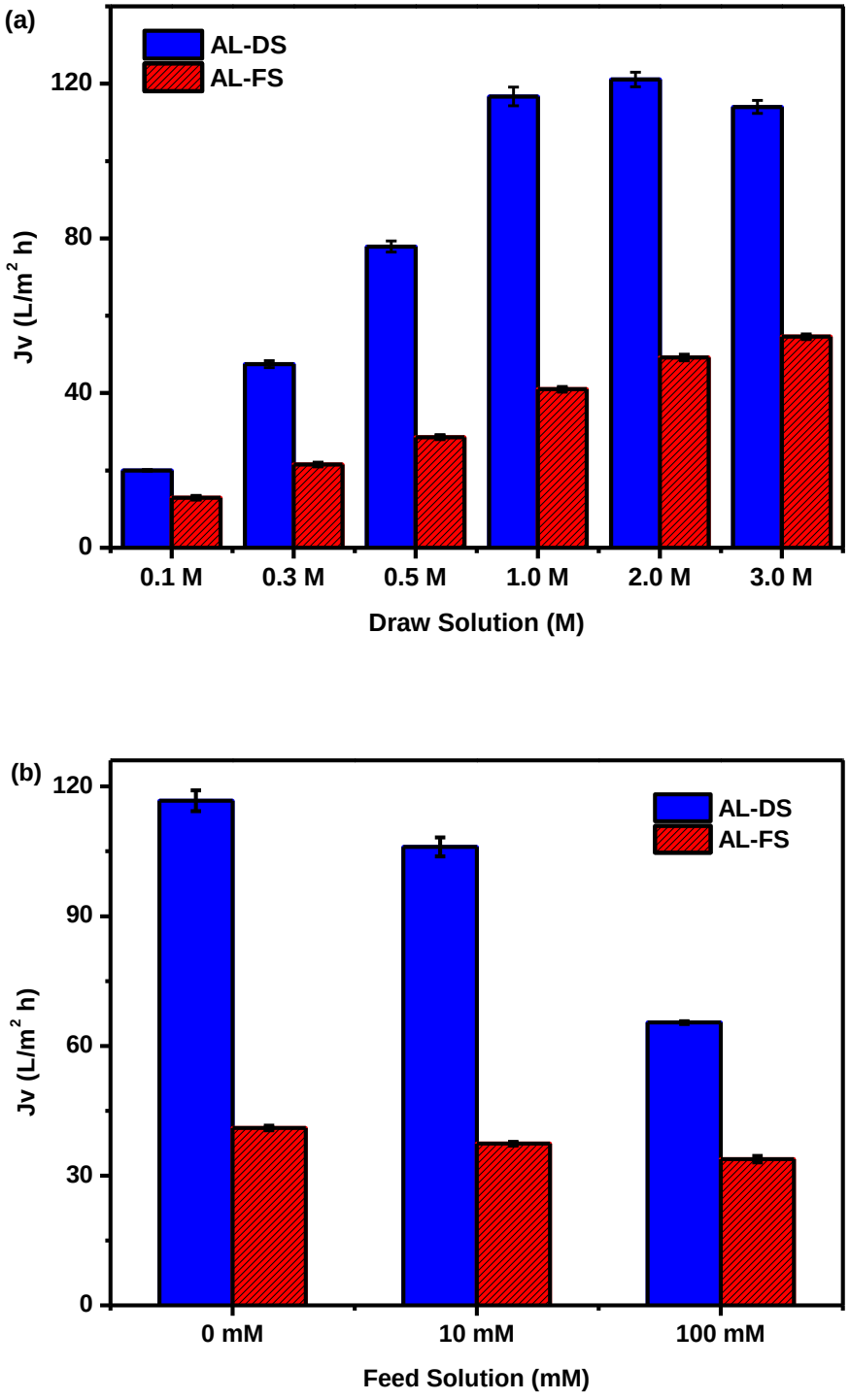


**Fig. 7.** Effect of draw solution and feed solution concentration on on FO water flux of SG-PAN MMMs (M1.00). (a) Effect of DS concentration (0.1 – 3.0 M $MgCl_2$) using DI water as FS; and (b) effect of FS concentration (0-100 mM NaCl) using 1 M $MgCl_2$) as DS. Error bar was based on the standard deviation of 3 replicate measurements.